ADVANCED ENERGY MATERIALS
www.advenergymat.de

Seasonality in Perovskite Solar Cells: Insights from 4 Years of Outdoor Data

Marko Remec, Mark Khenkin, Ulas Erdil, Quiterie Emery, Gopinath Paramasivam, Eva Unger, Rutger Schlatmann, Steve Albrecht, Marko Topič,* and Carolin Ulbrich*

Insights are reported from a 4-year outdoor study in Berlin using encapsulated p–i–n perovskite solar cells with the structure ITO | 2PACz | $Cs_{0.15}FA_{0.85}PbI_{2.55}Br_{0.45}$ (bandgap of 1.65 eV) | C_{60} | SnO_2 | Cu. Peak summer performance showed little to no degradation during the first two summers and only ≈2% absolute drop in outdoor power conversion efficiency from the first to fourth summer. Despite good stability, the devices exhibit significant seasonality, with winter performance up to 30% lower than in summer during the first year, increasing with aging. The factors contributing to this seasonality are separated into four categories: I) solar spectrum, II) device temperature, III) maximum power point tracking losses, and IV) metastability effects. Among these, metastability – particularly light-soaking behavior – is the largest contributing factor that sets perovskite technology apart from conventional photovoltaics. It was found that in cold, low-light winter conditions, voltage gains from light-soaking remain unsaturated, leading to reduced performance. Full saturation requires more than 24 h of continuous illumination, indicating that device performance depends on more than a single diurnal cycle. This comprehensive analysis highlights the complexity of seasonal behavior and the importance of long-term, real-world testing for accurate forecasting of perovskite photovoltaic energy yield.

1. Introduction

With major improvements in device performance during the last decade, small-area single-junction perovskite solar cells (PSCs) are now achieving power conversion efficiency (PCE) under standard test conditions (STC) of up to 26.95%.[1] Research focus is currently shifting from raising device efficiency toward upscaling and improving stability.[2] On the path to perovskite commercialization, understanding the long-term real-world behavior is particularly important, not only with respect to device reliability but in all aspects of their outdoor operation, to enable accurate prediction of energy yields and lifetime.

The power output of PV modules outdoors depends strongly on the weather conditions that differ from STC (25 °C, 1000 Wm^{-2}, AM1.5G). All established PV technologies exhibit slight seasonal changes with a periodic annual pattern. Real-world operating conditions have various effects depending on the type of solar cell (mostly on the absorber materials).[3] For the emerging perovskite PV devices, seasonal patterns have not been systematically analyzed yet, because until recently, no long-term outdoor datasets were available for these devices due to PSC stability issues.

Indoor experiments revealed that light cycling can introduce a wide range of possible PSC behaviors depending on the device structure.[4] These behaviors translate into metastable changes over the day-night cycle outdoors and significantly complicate the interpretation of outdoor data. Compared to the amount of data available from indoor stability experiments, outdoor datasets are still scarce,[5,6] Nevertheless, the first years-long outdoor datasets for perovskite-based solar cells are now becoming available,[4,7,8] This enables us to investigate the long-term

M. Remec, M. Khenkin, U. Erdil, Q. Emery, G. Paramasivam, E. Unger, R. Schlatmann, S. Albrecht, C. Ulbrich
Solar Energy Division
Helmholtz-Zentrum Berlin für Materialien und Energie
12489 Berlin, Germany
E-mail: mark.khenkin@helmholtz-berlin.de

The ORCID identification number(s) for the author(s) of this article can be found under https://doi.org/10.1002/aenm.202501906

DOI: 10.1002/aenm.202501906

M. Remec, M. Topič
Faculty of Electrical Engineering
University of Ljubljana
Ljubljana 1000, Slovenia
E-mail: marko.topic@fe.uni-lj.si

U. Erdil
Faculty of Chemistry
Bielefeld University
33615 Bielefeld, Germany

S. Albrecht
Fakultät Elektrotechnik und Informatik
Technische Universität Berlin
10587 Berlin, Germany

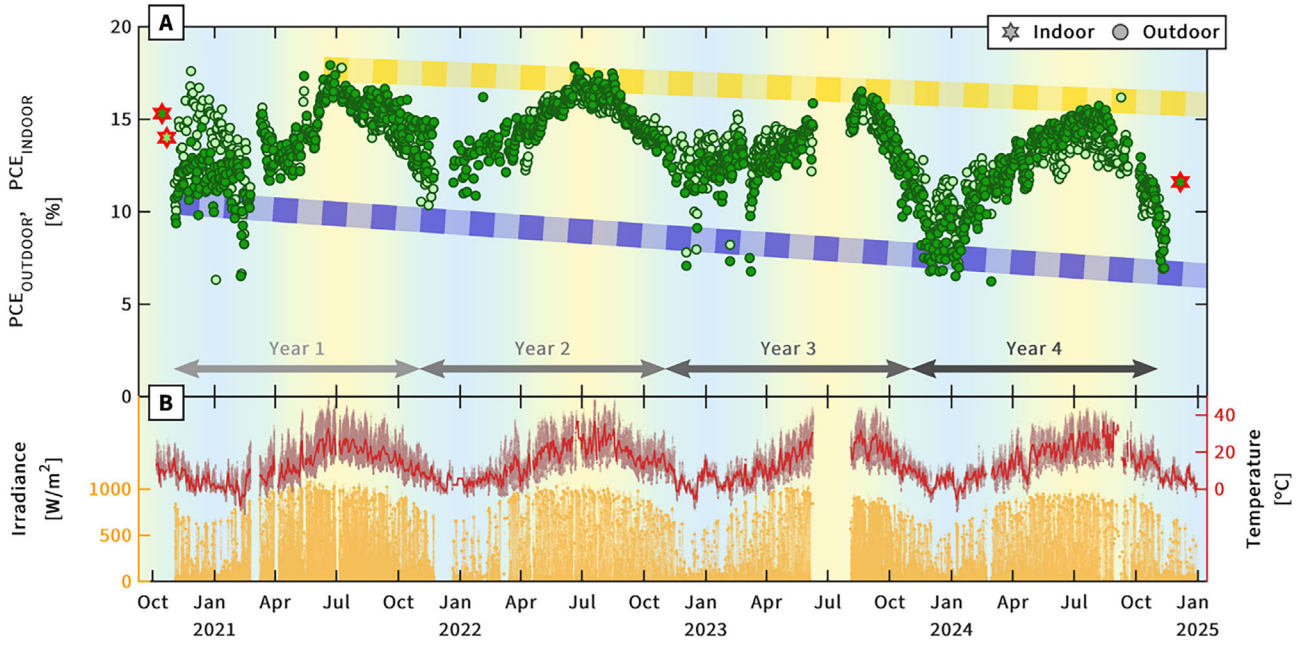

Figure 1. A) Long-term outdoor PCE for two 1 cm^2 single-junction perovskite devices with the same structure and encapsulation. Stars mark the PCE measured indoors at STC: initial PCE_{INDOOR} after encapsulation for both devices and PCE_{INDOOR} after 4 years of outdoor exposure for one fully light-soaked device. Yellow and blue dashed lines represent hypothetical linear degradation of 3% and 9% per year, as a guide to the eye for summer-to-summer and winter-to-winter changes in $PCE_{OUTDOOR}$. B) Temperature, measured on the back side of the device encapsulation, and irradiance in the plane-of-array. The background color gradient (on all outdoor graphs throughout this paper) represents the seasons – winter in blue, summer in yellow – and is shown to guide the eye. This dataset is an extension of the experiment previously reported in.[4,6]

performance of PSCs without degradation being the main factor determining their performance.

In this contribution, we present the analysis of our longest outdoor dataset for PSCs (**Figure 1**) that extends over 4 years for glass-glass laminated p–i–n perovskite solar cells with the structure of ITO | 2PACz | $Cs_{0.15}FA_{0.85}PbI_{2.55}Br_{0.45}$ | C_{60} | SnO_2 | Cu and a perovskite bandgap of 1.65 eV. The details of device fabrication are available in the Supporting Information, as described in.[6] Comparing peak summer $PCE_{OUTDOOR}$ values over the years shows little to no drop in outdoor performance during the first two summers and only a ≈2% absolute drop in outdoor power conversion efficiency ($PCE_{OUTDOOR}$) from the first to the fourth summer. These findings also apply to other devices that were tested in our outdoor field, although most other devices show more pronounced degradation (see Figure S5, Supporting Information), which overlaps with seasonal factors discussed here. It should be noted that the degradation rate of PSCs likely also depends on the season.[9] The initial part of this outdoor experiment was previously published to support the discussion on the topics of encapsulation[6] and indoor aging with cycled light.[4] Here, we utilize the extended data series to substantiate the discussion on pronounced seasonal changes observed in PSCs operated in Berlin. The devices shown are the most stable ones we have monitored outdoors; therefore, this dataset is well-suited for the discussion of seasonal effects. Instead of focusing on degradation-rate analysis, we discuss the factors affecting seasonal performance variations.

In Figure 1A, $PCE_{OUTDOOR}$ values represent the average daily performance outdoors. The value was calculated based on device power output and irradiance in the plane of the array, with no temperature or spectral mismatch correction applied. Temperature, measured on the back side of the device encapsulation, and irradiance in the plane-of-array are shown in Figure 1B. Additional weather data (humidity, air temperature, wind speed, and the amount of precipitation) are shown in Figure S4 (Supporting Information). Daily evolutions of MPP parameters for representative summer and winter days each year are shown in Figure S6 (Supporting Information).

Indoor measurements of fully light-soaked devices (PCE_{INDOOR}, measured at STC, shown as stars in Figure 1A), at the beginning and after 4 years of outdoor exposure, demonstrate relatively good stability of the device, with an initial PCE_{INDOOR} of 15.3% and 11.6% after aging and extended light soaking (see Figure S8 (Supporting Information) for current–voltage (*I*–*V*) measurements). Meanwhile, outdoor results highlight the extremely pronounced seasonal behavior. The high variability in performance is present from the beginning of the outdoor exposure, when the PSCs had not degraded yet. With aging, the seasonal behavior only becomes more pronounced. Yellow and blue dashed lines in Figure 1A represent hypothetical linear degradation of 3% and 9% per year, as a guide to the eye for summer-to-summer and winter-to-winter changes in $PCE_{OUTDOOR}$. Degradation measured indoors at STC was ≈24% after 4 years (presuming linear degradation, which corresponds to 6% per year). The difference between the degradation of PCE_{INDOOR} measured under STC (6% per year) and the apparent degradation of $PCE_{OUTDOOR}$ measured summer-to-summer (3% per year) and winter-to-winter (9% per year) is due to seasonal changes, as discussed below.

Generally, we can separate the factors that contribute to seasonality into different categories: 1) solar spectra, 2) cell temperature, and 3) device metastability. As energy yield is directly influenced by maximum power point (MPP) tracking losses, we also discuss those, specifically for the combination of the investigated devices and the selected MPP tracker.

We will first introduce how the above-mentioned parameters affect conventional PV and the theoretically expected seasonal behavior of perovskite and conventional solar cells. Then, we will discuss our data and how those expectations translate to the actual outdoor performance of single-junction perovskite solar cells.

2. Parameters that Affect Seasonality in PV

2.1. Solar Spectra

Spectral conditions are one of the main differences between aging experiments indoors and outdoors. While spectral conditions for indoor experiments are well-defined and constant – usually set to AM1.5G spectrum – in outdoor experiments, the solar spectral conditions change both daily and seasonally.[10] The spectral properties of the light source are important, as they, together with the spectral response (SR) of the solar cell, define the generated photocurrent. The short-circuit current density (J_{SC}) of the device is calculated as:

$$J_{SC} = \int SR(\lambda) \cdot E_0(\lambda)\ d\lambda \tag{1}$$

SR is defined by the device structure and limited by the bandgap of the absorber layer. Low-bandgap materials are less affected by spectral changes, since they can absorb photons over a wider wavelength range. Spectral changes instantly affect the current generated by the device.

Outdoor $E_0(\lambda)$ is defined by sunlight, attenuated by the air mass, and atmospheric conditions. To simplify, we can represent the spectral conditions with a single value – average photon energy (APE),[11–13] calculated using the equation:

$$APE = \frac{\int_a^b E(\lambda)\ d\lambda}{q \cdot \int_a^b \phi(\lambda)\ d\lambda} \tag{2}$$

where $E(\lambda)$ is the photon energy, $\phi(\lambda)$ is the photon flux at wavelength λ, and a and b are the limits of integration. Higher values of APE reflect blue-light-rich and lower red-light-rich spectra. The calculated APE value depends on the wavelength range used for the calculation. In this work, a wavelength range from 300 to 1050 nm was used to be comparable with other works. Spectral changes at a particular location over the day and year depend on multiple parameters, such as sun position and atmospheric conditions. Winter-to-summer variations in insolation are more pronounced farther away from the equator.[14] The test site for this research, located in Berlin (latitude 52.52° N), therefore experiences relatively large annual changes in solar spectrum.[15]

Compared to crystalline silicon (c-Si) or copper indium gallium selenide (CIGS) solar cells with spectral sensitivity in the range of ≈300 to 1100 nm, the spectral sensitivity of perovskites used in single-junction devices is much narrower – typically ≈300 to 800 nm. That means that the performance variations of PSCs due to spectral changes are analogous to those of high-bandgap absorbers, such as amorphous silicon (a-Si:H), which has a spectral sensitivity range of ≈300 to 750 nm. Devices with a narrow spectral sensitivity range are more sensitive to changes in the solar spectrum. For an a-Si:H module, typical variations in sunlight spectra can result in a ~10% change in short-circuit current (I_{SC}), while for c-Si, the same conditions change I_{SC} only by ≈4%.[16]

2.2. Cell Temperature

Generally, PV devices perform worse at higher operating temperatures due to the negative temperature coefficient of power (γ). γ is directly influenced by the temperature dependency of the bandgap. While the bandgap for most semiconductors decreases with temperature, it increases for perovskite semiconductors.[17,18] A slight decrease in J_{SC} at higher temperatures, related to a bandgap increase, was observed in fresh devices, similar to those shown in Figure 1 (see Figure S10, Supporting Information). Additionally, due to their wide bandgap, perovskites have a lower γ compared to silicon.[18] Typical reported γ values for commercial Si modules range from ≈−0.3% to −0.4%/°C, while for state-of-the-art modules it can reach −0.26%/°C.[19] For PSCs, the reported γ values range from −0.1% to −0.3%/°C.,[4,5]

It is important to note that γ in perovskites cannot be predicted by the bandgap or PCE value measured at room temperature, as temperature-dependent properties are not determined solely by the active perovskite layer but are also influenced by other device layers (ETL, HTL, contacts).[18] Additionally, temperature coefficients in perovskite devices do not necessarily follow a monotonic trend. A change in the slope of γ has been observed for carbon-based perovskite devices,[20] as well as for PCS stacks with spiro-OMeTAD HTL.[21]

For silicon solar cells, temperature has the most pronounced effect on seasonal behavior. Due to the negative γ, performance in summer (high temperatures) is expected to be worse than in winter (low temperatures) at the same irradiance.

2.3. Metastability

In this work, we use the term metastability to describe the reversible processes – improvement or degradation – that cause changes in device performance. Among more mature PV technologies, a-Si:H is known for its pronounced metastability effect—referred to as the Staebler-Wronski effect (SWE). SWE results in a decrease in device performance under illumination; however, the effect is reversed at elevated temperatures. This was hypothesized to be an important factor in explaining why a-Si:H was the only PV technology (prior to PSCs) to show seasonal variations, with peak performance during the summer.[22] a-Si:H modules also show better performance when installed in locations where they operate at higher average temperatures.[23]

The light-soaking effect (LSE) – i.e., improvement in device performance after exposure to light – has been observed in multiple PV technologies. However, depending on the technology, the effect can vary in magnitude and may either improve or

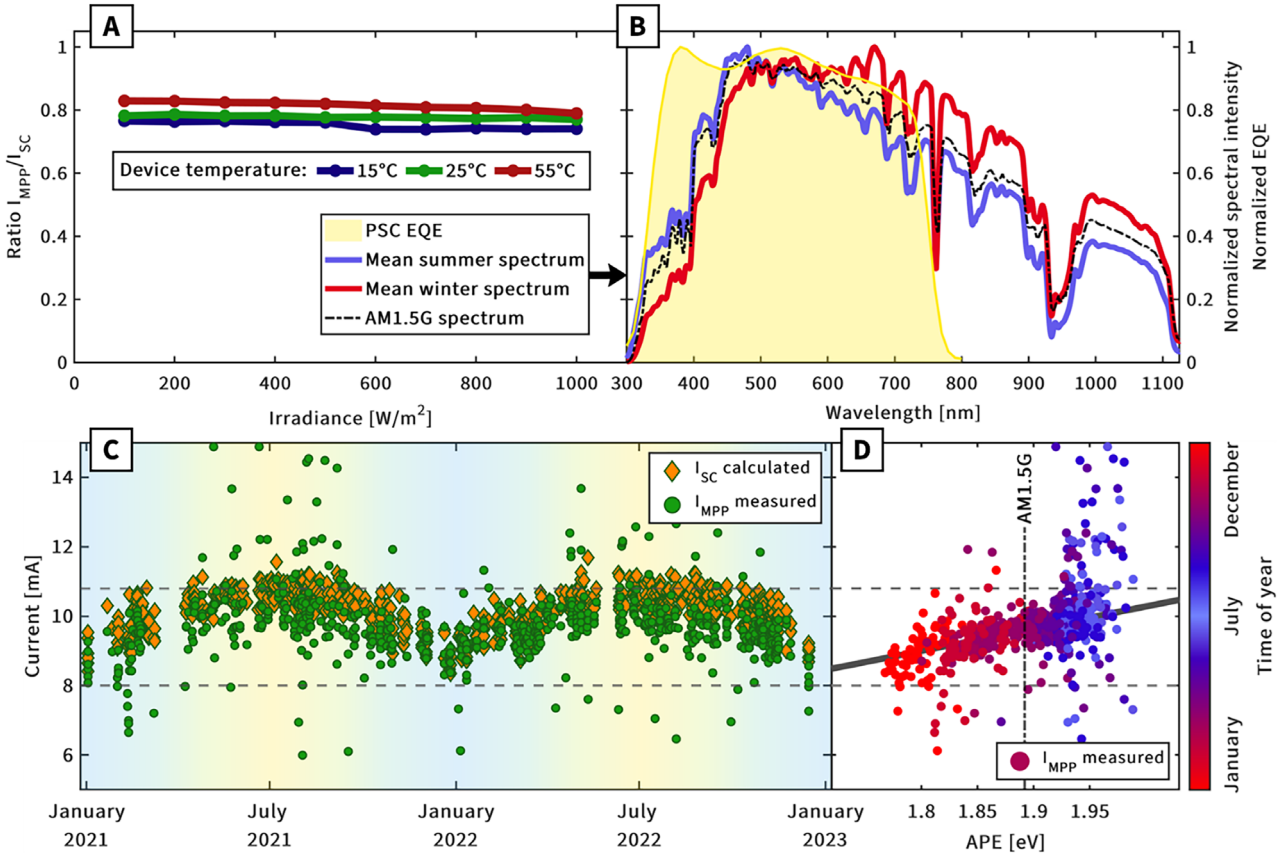

Figure 2. A) Ratio of I_{MPP}/I_{SCP} at different irradiance-temperature conditions. B) Normalized mean summer (blue) and winter (red) spectrum calculated for irradiances 500 ± 20 Wm^{-2}. AM 1.5G spectrum is marked with a dashed black line, and device EQE is shown as a yellow area. C) Variation of short-circuit current calculated from EQE and spectral data compared to measured outdoor I_{MPP} in the irradiance range 500 ± 20 Wm^{-2}. D) Spectral conditions as APE value for each I_{MPP} point in Figure 2C. Colors mark the season (red for winter and blue for summer), and the solid grey line represents linear regression between APE and I_{MPP}.

degrade device performance.[24] PSCs also exhibit reversible behavior over the day-night or light-dark cycle,[4,7] where the underlying mechanism is typically ionic movement. Depending on the PSC structure, both LSE-induced reversible increases and decreases in performance have been observed. The major difference from other PV technologies lies in how pronounced these effects are in PSCs.

3. Results

The devices were monitored in the outdoor test field in Berlin, Germany (Figure S3, Supporting Information). The conditions at the location differ significantly between seasons – with high irradiance and high temperatures in summer, and mostly diffuse, low irradiance light and low temperatures in winter (Figure S9, Supporting Information). These conditions are typical for northern Europe,[25] which is classified as "*DL*" zone in the Köppen–Geiger-Photovoltaic classification,[26] i.e., a temperate zone with low annual irradiation.

Some variation in performance is observable even when the devices are still in a "fresh" state – we can attribute this share to changes in operating conditions alone. The amplitude of other effects, such as metastability, increases with device degradation. These degradation-induced changes in the device dominantly affect the performance of aged devices.

We separated the contributions to seasonal variation in performance into the following categories:

1) Changes in spectral conditions.
2) Effect of temperature coefficients and cell operating temperature.
3) Hysteresis in the current density–voltage (*J*–*V*) characteristics and MPP tracking losses.
4) Perovskite metastability: reversible and irreversible degradation.

3.1. Contributions to Seasonality

3.1.1. Changes in Spectral Conditions

The spectrum in the plane of the array at the outdoor field is measured periodically every 5 minutes. Data show that the spectral conditions are blue-rich in summer and red-rich in winter (Figure S7, Supporting Information). **Figure** 2B shows normalized mean summer (blue line) and mean winter (red line) spectra, calculated for irradiances of 500 ± 20 Wm^{-2}. The selected

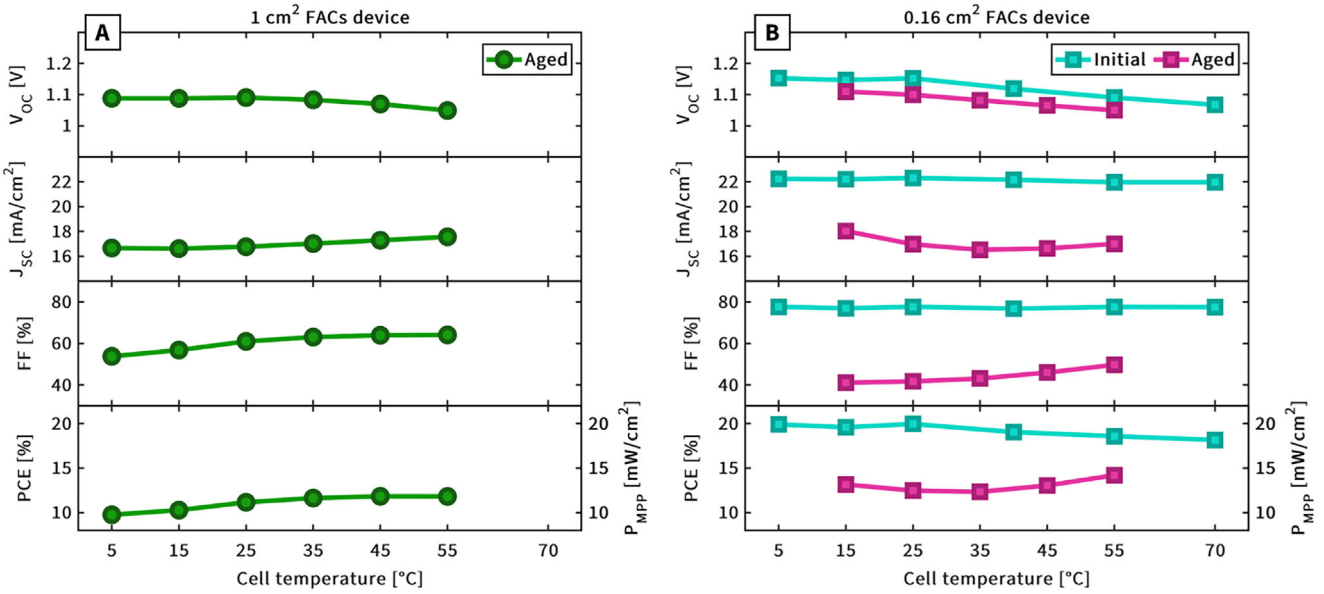

Figure 3. Performance of completely light-soaked PSCs at different temperatures. A) The 4-year-old device shown in Figure 1, and B) a smaller (0.16 cm^2) device with the same device stack. Measurements were taken after encapsulation (initial) and after 2 years of outdoor operation (aged) – see the outdoor data of this experiment in Figure S5 (Supporting Information).

irradiance range was chosen to obtain an adequate number of data points at the same irradiance under different conditions throughout the year. Both summer and winter spectra differ from the reference AM1.5G spectrum, marked in Figure 2B with a dashed black line. The yellow area in Figure 2B represents the external quantum efficiency (EQE) for one of the PSC devices measured after encapsulation. Using the device EQE, we can calculate the theoretical I_{SC} of the device based only on spectral irradiance. Based on PCE values (Figure 1A), we assume that the EQE does not change significantly during the first two years of outdoor operation.

To compare the calculated I_{SC} with the outdoor-measured maximum power point current (I_{MPP}), we first confirmed through indoor measurements – using a solar simulator and different irradiance levels (AM1.5G spectrum) at controlled temperatures (15, 25, and 55 °C) – that the ratio I_{MPP}/I_{SC} (shown in Figure 2A) does not change considerably under different operating conditions. Therefore, we can conclude that changes in current due to spectral variation are reflected equally in both I_{SC} and I_{MPP}.

The first two years of I_{MPP} data (green circles) for the irradiance range of 500 ± 20 Wm^{-2} are shown in Figure 2C, together with the calculated I_{SC} data points (orange diamonds). As the seasonal variation is the same for the measured and calculated current, we can attribute the change in I_{MPP} to changes in spectral conditions. The difference between summer and winter current values can exceed 10% at the same irradiance. Approximate minimum and maximum values of I_{MPP} are marked with dashed grey lines as a guide to the eye.

Spectral conditions at the time of each I_{MPP} data point in Figure 2C are shown in Figure 2D. There is a clear correlation between I_{MPP} and APE values – a solid gray line represents the linear regression. Point colors indicate the season, with red representing winter and blue representing summer. As in Figure 2B, summer and winter conditions are clearly separated, forming two distinct clusters, neither of which coincides with the reference AM1.5G spectrum in the middle (marked with a vertical dashed line).

Summarizing, comparing the same irradiance levels, the seasonal differences in solar spectra affect the current generated by the solar cell. Blue-light-rich summer conditions allow PSCs to generate more current compared to winter, with the difference in I_{MPP} reaching up to 10% between mean winter and summer values.

3.1.2. Effect of Temperature Coefficients and Cell Operating Temperature

The low temperature coefficients of power (γ) observed in PSCs, compared to other PV technologies, suggest that PSCs perform relatively better under high-temperature conditions during summer.

For the aged, four-year-old device, the temperature coefficients were found to differ considerably from expectations. **Figure 3A** demonstrates the performance parameters measured indoors at different temperatures and 1 sun irradiance (AM1.5G). The selected temperature range reflects the typical outdoor temperatures of the devices exposed at our test field in Berlin. While the open-circuit voltage (V_{OC}) decreases with higher temperatures as expected, the fill factor (FF) shows considerable improvement – i.e., a positive temperature coefficient (T_C). The PCE trend follows the FF, with higher values at high temperatures.

To illustrate the effect of outdoor aging on temperature coefficients, we show in Figure 3B measurements on both the initial (after encapsulation) and the aged device, with slightly different perovskite stoichiometry but the same device stack (see Supporting Information for device fabrication). The active area of this

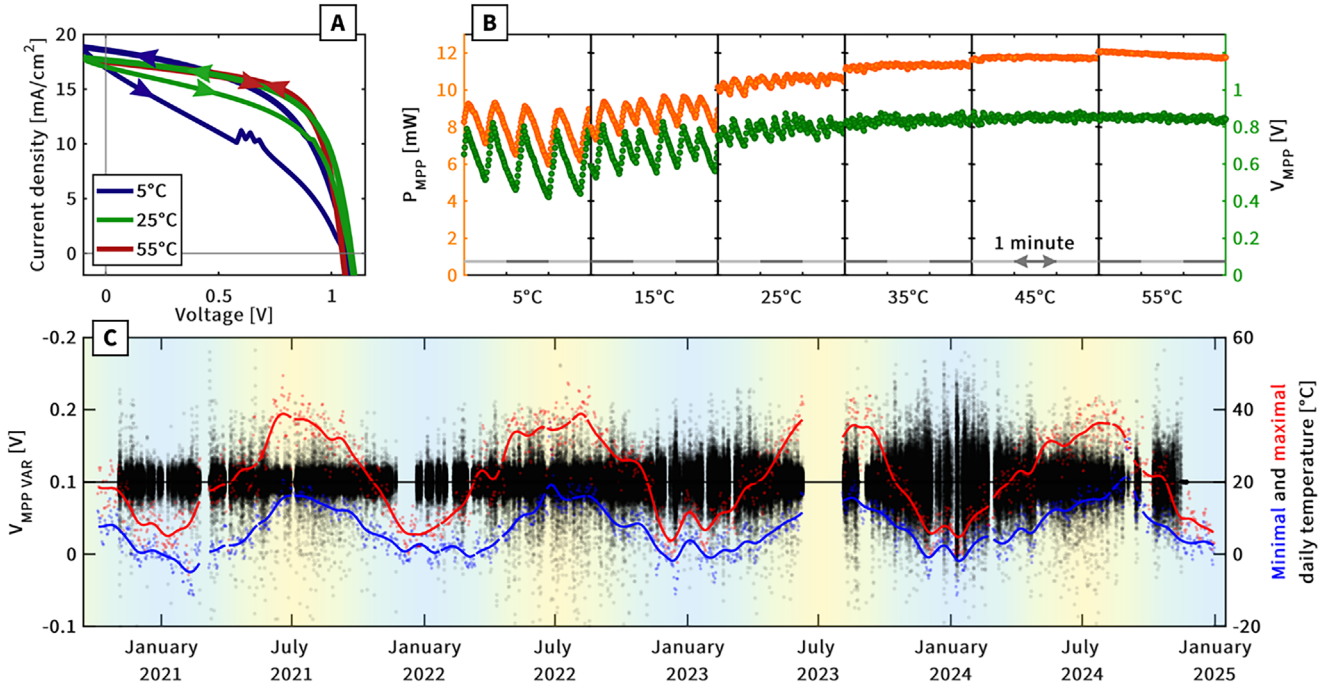

Figure 4. A) *J–V* measurements in forward and reverse scan directions of the 4-year-old device measured at different operating temperatures. B) Indoor MPP tracking for the same device, at different temperatures and light intensity of 1000 Wm^{-2}. C) Outdoor V_{MPP} variance (data for irradiance values below 100 Wm^{-2} was filtered; see Figure S14, Supporting Information). Blue and red lines show average minimum and maximum daily temperatures.

solar cell was smaller, 0.16 cm^2. The device was also aged outdoors, although for a shorter period (approximately two years) – see Figure S5 (Supporting Information) for details. Measurements on fresh devices show that γ is only slightly negative, due to the drop in V_{OC} at high temperatures. PCE decreases from 19.9% at 5 °C to 18.1% at 70 °C. In contrast to the fresh device, where γ follows the V_{OC} trend, the PCE of the aged device follows the FF trend. Unlike for V_{OC}, where the temperature behavior is defined by the active perovskite layer, changes in FF of aged cells are most likely connected to the increase of mobile ions concentration,[27,28] or temperature-activated transport in the charge transport layers,[17,29]

The γ contribution to seasonality differs between fresh and degraded devices. Considering only temperature effects, fresh devices lose performance in summer compared to winter due to higher operating temperatures and a negative γ. For degraded devices, however, changes in the temperature coefficients of the fill factor and short-circuit current improve the overall performance at higher operating temperatures, thereby giving them a "summer boost."

3.1.3. J–V Hysteresis and MPP Tracking Losses

A temperature-irradiance performance matrix was measured for one of the aged, four-year-old devices. Before performance matrix measurements, the device was light-soaked under constant 1 sun equivalent illumination to eliminate the transient effects (will be discussed below). During the performance matrix measurements, the device was connected to an MPP tracker. At each operating condition, once the MPP tracking stabilized, *I–V* measurements were performed. Measurements were conducted over a temperature range from 5 to 55 °C in 10 °C steps. At each temperature, irradiance was changed from 1000 to 100 Wm^{-2} in 100 Wm^{-2} steps.

Figure 4A shows current density–voltage (*J–V*) curves measured at 1000 Wm^{-2} and three different temperatures: 5, 25, and 55 °C (blue, green, and red lines, respectively). There is a pronounced effect of temperature on *J–V* hysteresis. At 55 °C, the hysteresis is negligible; the FF does not change depending on the *J–V* scan direction (forward or reverse). In contrast, at 5 °C, the FF of the forward *J–V* scan is significantly lower. As shown in Figure S8 (Supporting Information), the device in its fresh state did not exhibit *J–V* hysteresis at room temperature (and the same *J–V* scan parameters). This increase in *J–V* hysteresis after outdoor exposure (Figure 4A) might originate from internal electric field screening, likely caused by aging-induced increase in mobile ion concentration,[27,28] Reduced *J–V* hysteresis at higher operating temperatures has also been observed for fresh devices in the literature,[30–33]

J–V hysteresis is common in perovskite devices, and it has already been shown that it also affects MPP tracking quality.[34] Figure 4B shows power (P_{MPP}) and voltage (V_{MPP}) at maximum power point during 3 minutes of MPP tracking at 1 sun irradiance for each measured temperature. The same µMPP tracker used in the outdoor setup was implemented for indoor MPP tracking. In both cases, the tracking algorithm used was "perturb and observe" (P&O), with a period of 200 ms and a voltage step of 6 mV.

The quality of MPP tracking at higher temperatures (35, 45, and 55 °C) is good, as there is almost no variance in P_{MPP} and only small perturbations in V_{MPP}. That confirms that both the

MPP tracker and the selected algorithm are suitable for the device under observation, i.e., only small deviations of the device voltage from its actual V_{MPP} are expected due to the use of P&O algorithm. At low temperatures, however, V_{MPP} (and with it P_{MPP}) begins to fluctuate significantly compared to higher temperatures. In the worst case, at 5 °C, the V_{MPP} fluctuates between 0.4 and 0.8 V. That means that the MPP tracker is searching for the correct MPP across a range exceeding 35% of the device voltage. High fluctuations in voltage also cause tracking losses, i.e., energy loss when the device operates outside its actual maximum power point due to non-optimal tracking algorithm parameters. Outdoors, this results in lower energy yield at lower operating temperatures.

Figure S11 (Supporting Information) shows *P*–*V* characteristics measured with different scan speeds at each temperature, together with MPP tracking values. It visualizes where in *P*–*V* characteristic the MPP tracker is searching for the MPP and how high hysteresis at low temperatures negatively affects the quality of the tracking.

Variance in MPP tracking voltage ($V_{MPP\ VAR}$) was also calculated for outdoor data shown in Figure 1 (see Figures S12 and S13, Supporting Information, for the definition of this parameter). Figure 4C shows $V_{MPP\ VAR}$ together with daily minimum and maximum temperatures of the device. In the first two years, the amplitude of $V_{MPP\ VAR}$ is small, with little variation between seasons. This indicates adequate operation of the chosen MPP tracking system and algorithm for fresh devices. In the following two years, when the device is more degraded, the difference in $V_{MPP\ VAR}$ between summer (higher temperatures) and winter (lower temperatures) becomes more pronounced. This corresponds to the behavior observed in indoor measurements, where MPP tracking quality is worse at low temperatures due to increased *J*–*V* hysteresis. Although different MPP tracking parameters (such as algorithm, period, and voltage step) might improve the MPP tracking of the aged device, the parameters were kept constant throughout the outdoor experiment for consistency.

Exhibiting such behavior – with the observed dramatic decrease in MPP tracking quality at low temperatures – leads to higher MPP tracking losses (and hence lower energy yield) in winter compared to summer for PSCs. Such effects should be considered part of device degradation, even if they do not affect the steady-state device PCE under standard test conditions.

3.1.4. Perovskite Metastability

Metastability in PSCs includes not only effects that are reversible on the timescale of a single day,[35] but, based on our results, also changes that occur over much longer time periods.[4] Regardless of the timescale, most of the effects are caused by ion movement in the perovskite layer.[36,37] With aging, metastability often becomes more pronounced, as is the case for the aged device presented here. While fresh devices reached light-soaking saturation (1 sun, 25 °C) within several minutes, after four years of operation, the examined solar cell required several days of continuous light-soaking (1 sun, 25 °C) to reach its maximum performance. The recovery process – in this case due to the LSE (described in detail in[7]) – is affected by both irradiance and temperature.

For studied devices, V_{OC} and V_{MPP} are the main parameters that change during the light-soaking (see Figure S8, Supporting Information). To investigate the seasonal impact of metastability (**Figure 5D**), we monitored V_{OC} and V_{MPP} of the aged device during prolonged light-soaking and dark storage periods. It should be emphasized that for such metastable devices, preconditioning is a critical factor, as it directly and significantly affects the measured performance. For the light-soaking measurements presented in Figure 5A–C, the device was taken indoors in December and was therefore in its winter state. To further "reset" any prior light-soaking effects, the device was kept in dark storage for several days before the start of the experiment.

Figure 5A shows the recovery of V_{OC} and V_{MPP} under constant 1 sun equivalent illumination, starting from the dark storage (winter) state. The device was placed on a temperature-controlled stage and connected to an MPP tracker, with *I*–*V* measurements taken periodically. Voltages shown in Figure 5A–C were extracted from the reverse *I*–*V* scans.

During the first part of the experiment (Figure 5A), when the device was held at 25 °C, we observed a continuous increase in both V_{OC} and V_{MPP}. While the increase is quite rapid during the first 12 h, even after 60 h, V_{MPP} still did not reach the values measured outdoors during the previous (2023) summer. Keeping the same irradiance, the operating temperature was increased to 40 °C – representing typical summer temperature conditions outdoors (Figure 5B). The increase in temperature caused the voltage values to increase further, with V_{MPP} beginning to stabilize after 12 h at the elevated temperature (in addition to the 60 h under 1 sun at 25 °C). In the "saturated" light-soaked state, the measured V_{OC} was comparable to that of a fresh device (Figure S8, Supporting Information), and V_{MPP} matched the value reached outdoors in summer.

Once the device reached its best performance, the conditions were changed to "dark storage," simulating the low-irradiance conditions of winter (Figure 5C). The operating temperature was set back to 25 °C. To monitor device performance, short periodic light pulses (1 sun equivalent) were used to measure *I*–*V* characteristics. Figure 5C shows that the voltage values dropped significantly immediately after continuous illumination stopped. Although most of the change occurred in the first 12 h, the voltages continued to decrease slowly for more than 72 h before reaching the "winter levels" (blue line in Figure 5A–C).

Although V_{MPP} is affected by both temperature and irradiance, the changes due to these factors are minor compared to the magnitude of metastability effects shown. We can therefore attribute most of the changes in the "daily mean V_{MPP}" shown in Figure 5D to metastability – e.g., an unsaturated light-soaking state.

Yellow and blue horizontal lines in Figure 5 mark the maximum and minimum V_{MPP} values measured indoors. The maximum value (yellow line) matches well with the summer outdoor values in Figure 5D, both during the first summer (2021) and even the last summer, four years later. The minimum value (blue line), on the other hand, is much lower than what was observed outdoors in the first (2021) or second (2022) winter. However, the aged, more degraded device reaches similarly low outdoor V_{MPP} values in the winter of 2024.

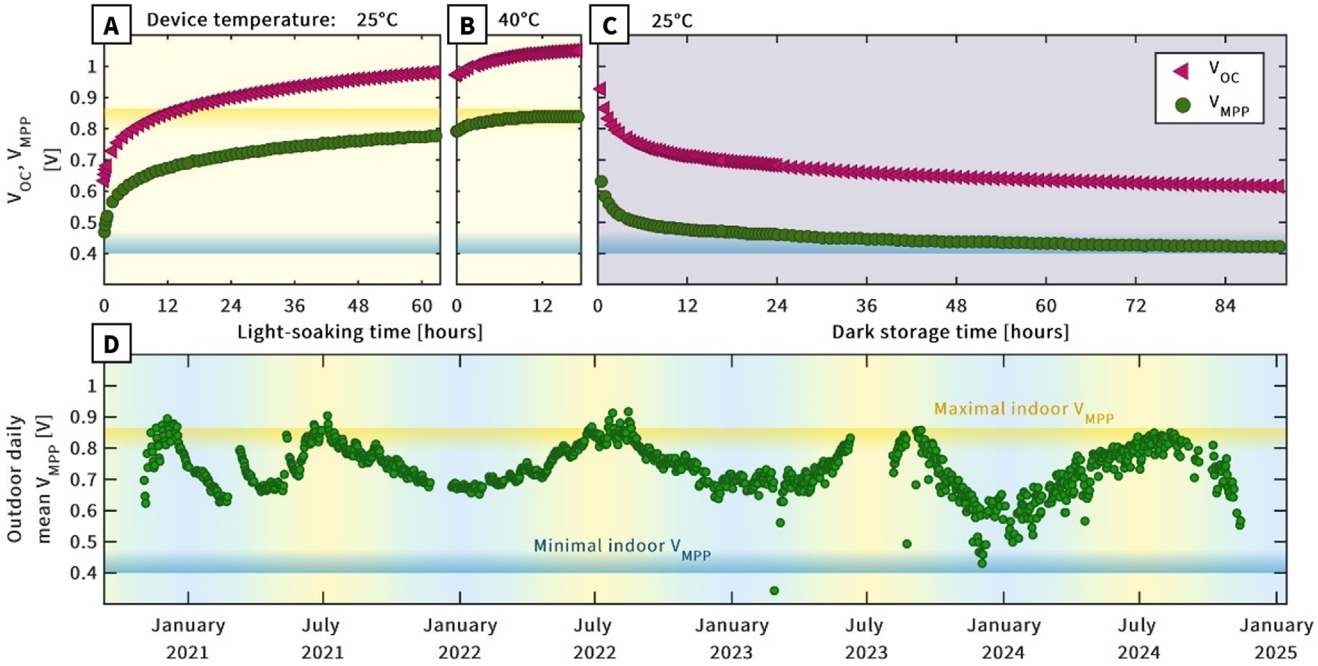

Figure 5. A–C) Indoor light-soaking (1 sun equivalent illumination)/dark storage at different temperatures for the 4-year-old device taken indoors in winter. (A) First, the device was light-soaked for 60 h at 25 °C, which was not sufficient to saturate the LSE. (B) Continued light-soaking with the temperature increased to 40 °C, leading to saturation in the next 12 h. (C) Subsequent dark storage resulted in a voltage decrease back to the initial values; however, another 72 h were needed to reach "dark storage" voltage values (as measured at the beginning of light-soaking). D) Outdoor daily mean V_{MPP} values throughout four years. The high/low V_{MPP} values correspond to full saturation/full loss of the LSE in the indoor experiment. Characteristic summer and winter V_{MPP} values from the outdoor experiment are marked with yellow and blue lines.

The experiment shows that for degraded perovskite devices, metastable effects, such as light-soaking, can last significantly longer than a single day-night cycle. We were able to condition the device from its winter state with $V_{MPP} = 0.5$ V to its summer state with $V_{MPP} = 0.85$ V, but it took 72 continuous hours under illumination and 72 h in the dark (and it would have taken longer had the temperature not been increased). This explains the contribution of metastability to the seasonality observed – generally, devices are more light-soaked during summer (see summer-to-winter irradiation difference in Figure S9B, Supporting Information), which is beneficial to the performance.

4. Discussion

The magnitude of seasonal changes is expected to be both climate-specific and device-specific for perovskite PV. However, the fact that it can reach such a high magnitude, as shown here for the case of Berlin, even for decently stable devices, challenges the conventional approaches to outdoor stability evaluation. For example, the cells shown in Figure 1 would drop below the T_{80} line every winter and "recover" their performance during the following spring and summer. Furthermore, while the first-to-fourth summer $PCE_{OUTDOOR}$ peak difference is less than 15%, the first-to-fourth winter $PCE_{OUTDOOR}$ values drop by ≈40% (see Figure 1A). This suggests that in experiments shorter than a year, the impacts of seasonal changes and device degradation can overlap and create uncertainty.

The extrapolation of conclusions to other climates is complex, as the discussed factors affecting seasonality interact with each other. Compared to Berlin, locations closer to the equator experience less pronounced seasonal spectral variation due to the impact of latitude on seasonal air mass variation. Therefore, the relatively high changes in generated current due to spectral shifts observed at our location would be reduced in more equatorial locations.[15] Based on the changes in temperature coefficients observed for fresh and aged devices, the device performance in hot climates would be worse initially, but the poor performance and MPP tracking losses in aged devices at low temperatures might be mitigated. These effects would likely increase in magnitude in locations with warmer climates and high annual temperature variation. Seasonal variations also affect light-soaking, the dominant metastable effect for the devices presented. Light-soaking losses in locations with high insolation and ambient temperatures throughout the year can be more than twice as low compared to locations with less favorable conditions.[7]

Thorough indoor experiments are required for sound conclusions on the outdoor lifetime of PSCs. On the other hand, the extent of metastability (even for rather stable devices) challenges the established practice of quantifying the outdoor device stability using only "normal" *I–V* curves measured under STC indoors. By "normal," we refer to *I–V* measurements that do not last for a full week, such as those shown in Figure 5A–C. To the best of our knowledge, good scientific practices for the outdoor evaluation of highly metastable devices are still under discussion in the community, and extensive

research is needed to deepen our understanding of PSCs and to facilitate the quick and confident adoption of perovskite technology.

Great care in the preconditioning of PSCs is required when performing indoor measurements, especially for aged devices. As shown in Figure 5, the time needed to fully saturate the LSE may exceed one day – which is not convenient (or even feasible) for intermediate indoor characterization of devices during outdoor experiments.

5. Conclusion

In this contribution, we presented results from the longest (4-year-long) outdoor dataset currently available (to the best of our knowledge) for perovskite solar cells. Peak summer outdoor performance shows little to no drop during the first two summers and less than a 15% relative decrease between the first and fourth summer. Despite the good summer-to-summer stability of the devices, the seasonality observed in the Berlin climate is significantly more pronounced compared to conventional PV technologies. It is expressed as up to 30% better performance of perovskite cells in summer compared to winter (or even more so for aged cells). This behavior of PSCs was interpreted by separating and explaining the different contributing factors.

Seasonal changes in the solar spectrum – leading to blue-light-rich summers and red-light-rich winters at our location – can result in a 10% difference in generated current between seasons at the same irradiance levels. Changes in the operating temperature affect the observed PSCs in different ways depending on the state of the device, with initially negative temperature coefficients becoming positive in degraded devices. Additionally, device metastability, with the LSE as the dominant behavior in the observed devices, results in lower device voltage during cold, low-light winter conditions and becomes more pronounced as the device ages. During operation in real-world conditions, MPP tracking losses also need to be considered. In the PSCs studied, these losses are linked to the magnitude of *J–V* hysteresis, which increases significantly in aged devices and at low operating temperatures. As a result, the energy yield of the observed devices is reduced during the third and fourth winters.

Overall, the presented long-term outdoor data for the lab-scale PSC devices demonstrates the potential of this technology to reach the operational lifetime requirements of current commercialized PV technologies. However, it is important to improve our understanding of the processes behind their unique real-world behavior to achieve accurate data interpretation and energy yield forecasting – and to potentially reduce the magnitude of seasonal variations in performance through device optimization.

Supporting Information

Supporting Information is available from the Wiley Online Library or from the author.

Acknowledgements

M.R., M.K., and C.U. acknowledge the support of the European partnering project TAPAS (PIE-0015). M.R. and U.E. acknowledge the support of the Helmholtz Association under the project Zeitenwende – Tandem Solarzellen. M.R. and M.T. acknowledge the support of the Slovenian Research and Innovation Agency (ARIS) under the program P2-0415. U.E. further acknowledges support from the German-Israeli Helmholtz International Research School HI-SCORE (HIRS-0008). This project is co-funded by the European Union, the PEPPERONI project, no. 101084251. Views and opinions expressed are, however, those of the author(s) only and do not necessarily reflect those of the European Union or the European Climate, Infrastructure and Environment Executive Agency (CINEA). Neither the European Union nor the granting authority can be held responsible for them.

Conflict of Interest

The authors declare no conflict of interest.

Data Availability Statement

The data that support the findings of this study are available from the corresponding author upon reasonable request.

Keywords

MPP tracking, outdoor, perovskite solar cells, seasonality, stability

Received: April 4, 2025
Revised: June 16, 2025
Published online: July 7, 2025

[1] Best Research-Cell Efficiency Chart | Photovoltaic Research | NREL, https://www.nrel.gov/pv/cell-efficiency.html (accessed: February 2007).
[2] S.-P. Feng, Y. Cheng, H.-L. Yip, Y. Zhong, P. W. K. Fong, G. Li, A. Ng, C. Chen, L. A. Castriotta, F. Matteocci, L. Vesce, D. Saranin, A. D. Carlo, P. Wang, J. Wei Ho, Y. Hou, F. Lin, A. G. Aberle, Z. Song, Y. Yan, X. Chen, Y. M. Yang, A. A. Syed, I. Ahmad, T. Leung, Y. Wang, J. Lin, A. M. C. Ng, Y. Li, F. Ebadi, et al., *J. Phys. Mater.* **2023**, *6*, 032501.
[3] A. Louwen, A. C. de Waal, R. E. I. Schropp, A. P. C. Faaij, W. G. J. H. M. van Sark, *Prog. Photovoltaics* **2017**, *25*, 218.
[4] M. V. Khenkin, H. Köbler, M. Remec, R. Roy, U. Erdil, J. Li, N. Phung, G. Adwan, G. Paramasivam, Q. Emery, E. Unger, R. Schlatmann, C. Ulbrich, A. Abate, *Energy Environ. Sci.* **2024**, *17*, 602.
[5] M. Jost, B. Lipovsek, B. Glazar, A. Al-Ashouri, K. Brecl, G. Matic, A. Magomedov, V. Getautis, M. Topic, S. Albrecht, *Adv. Energy Mater.* **2020**, *10*, 2000454.
[6] Q. Emery, M. Remec, G. Paramasivam, S. Janke, J. Dagar, C. Ulbrich, R. Schlatmann, B. Stannowski, E. Unger, M. Khenkin, *ACS Appl. Mater. Interfaces.* **2022**, *14*, 5159.
[7] M. Remec, Š. Tomšič, M. Khenkin, Q. Emery, J. Li, F. Scheler, B. Glažar, M. Jankovec, M. Jošt, E. Unger, S. Albrecht, R. Schlatmann, B. Lipovšek, C. Ulbrich, M. Topič, *Adv. Energy Mater.* **2024**, *14*, 2304452.
[8] V. Paraskeva, M. Norton, A. Livera, A. Kyprianou, M. Hadjipanayi, E. Peraticos, A. Aguirre, S. Ramesh, T. Merckx, R. Ebner, T. Aernouts, A. Krishna, G. E. Georghiou, *ACS Energy Lett.* **2024**, *9*, 5081.
[9] R. K. Gupta, D. K. Kumar, V. Sudhakar, J. M. Beckedahl, A. Abate, E. A. Katz, I. Visoly-Fisher, *Adv. Energy Mater.* **2025**, *15*, 2403844.
[10] G. S. Kinsey, N. C. Riedel-Lyngskær, A.-A. Miguel, M. Boyd, M. Braga, C. Shou, R. R. Cordero, B. C. Duck, C. J. Fell, S. Feron, G. E. Georghiou, N. Habryl, J. J. John, N. Ketjoy, G. López, A. Louwen, E. L. Maweza, T. Minemoto, A. Mittal, C. Molto, G. Neves, G. N. Garrido, M. Norton, B. R. Paudyal, E. B. Pereira, Y. Poissant, L. Pratt, Q. Shen, T. Reindl, M. Rennhofer, et al., *Renewable Energy* **2022**, *196*, 995.

[11] T. Minemoto, Y. Nakada, H. Takahashi, H. Takakura, *Sol. Energy* **2009**, *83*, 1294.
[12] D. Dirnberger, G. Blackburn, B. Müller, C. Reise, *Sol. Energy Mater. Sol. Cells* **2015**, *132*, 431.
[13] G. A. Farias-Basulto, M. Á. Sevillano-Bendezú, M. Riedel, M. Khenkin, J. A. Töfflinger, R. Schlatmann, R. Klenk, C. Ulbrich, *Sol. Energy* **2023**, *266*, 112175.
[14] J. C. H. Chiang, A. J. Broccoli, *Geosci. Lett.* **2023**, *10*, 58.
[15] M. A. Sevillano-Bendezú, M. Khenkin, G. Nofuentes, J. de la Casa, C. Ulbrich, J. A. Töfflinger, *Sol. Energy* **2023**, *259*, 174.
[16] A. Virtuani, L. Fanni, *Prog. Photovoltaics* **2014**, *22*, 208.
[17] O. Dupré, R. Vaillon, M. A. Green, *Sol. Energy Mater. Sol. Cells* **2015**, *140*, 92.
[18] T. Moot, J. B. Patel, G. McAndrews, E. J. Wolf, D. Morales, I. E. Gould, B. A. Rosales, C. C. Boyd, L. M. Wheeler, P. A. Parilla, S. W. Johnston, L. T. Schelhas, M. D. McGehee, J. M. Luther, *ACS Energy Lett.* **2021**, *6*, 2038.
[19] "Hi-MO 9," Longi Hi-MO 9, https://www.longi.com/en/products/modules/hi-mo-9/ (accessed: March 2025).
[20] S. Bhandari, A. Roy, A. Ghosh, T. K. Mallick, S. Sundaram, *Sustain. Energy Fuels* **2020**, *4*, 6283.
[21] W. Tress, K. Domanski, B. Carlsen, A. Agarwalla, E. A. Alharbi, M. Graetzel, A. Hagfeldt, *Nat. Energy* **2019**, *4*, 568.
[22] A. Phinikarides, G. Makrides, B. Zinsser, M. Schubert, G. E. Georghiou, *Renewable Energy* **2015**, *77*, 51.
[23] R. Ruther, J. del Cueto, G. Tamizh-Mani, A. A. Montenegro, S. Rummel, A. Anderberg, In *2008 33rd IEEE Photovoltaic Specialists Conf.*, IEEE, Piscataway, NJ **2008**, pp. 1–5.
[24] M. Gostein, L. Dunn,In *2011 37th IEEE Photovoltaic Specialists Conf.*, IEEE, Piscataway, NJ **2011**, pp. 003126–003131.
[25] B. R. Paudyal, S. G. Somasundaram, A. Louwen, A. H. M. E. Reinders, W. G. J. H. M. van Sark, D. Stellbogen, C. Ulbrich, A. G. Imenes, *Renewable Energy* **2024**, *224*, 120057.
[26] J. Ascencio-Vásquez, K. Brecl, M. Topič, *Sol. Energy* **2019**, *191*, 672.
[27] J. Thiesbrummel, S. Shah, E. Gutierrez-Partida, F. Zu, F. Peña-Camargo, S. Zeiske, J. Diekmann, F. Ye, K. P. Peters, K. O. Brinkmann, P. Caprioglio, A. Dasgupta, S. Seo, F. A. Adeleye, J. Warby, Q. Jeangros, F. Lang, S. Zhang, S. Albrecht, T. Riedl, A. Armin, D. Neher, N. Koch, Y. Wu, V. M. Le Corre, H. Snaith, M. Stolterfoht, *Nat. Energy* **2024**, *9*, 664.
[28] S. Shah, F. Yang, E. Köhnen, E. Ugur, M. Khenkin, J. Thiesbrummel, B. Li, L. Holte, S. Berwig, F. Scherler, P. Forozi, J. Diekmann, F. Peña-Camargo, M. Remec, N. Kalasariya, E. Aydin, F. Lang, H. Snaith, D. Neher, S. De Wolf, C. Ulbrich, S. Albrecht, M. Stolterfoht, *Adv. Energy Mater.* **2024**, *14*, 2400720.
[29] S. Shao, J. Liu, H.-H. Fang, L. Qiu, G. H. ten Brink, J. C. Hummelen, L. J. A. Koster, M. A. Loi, *Adv. Energy Mater.* **2017**, *7*, 1701305.
[30] Y. Chen, S. Tan, N. Li, B. Huang, X. Niu, L. Li, M. Sun, Y. Zhang, X. Zhang, C. Zhu, N. Yang, H. Zai, Y. Wu, S. Ma, Y. Bai, Q. Chen, F. Xiao, K. Sun, H. Zhou, *Joule* **2020**, *4*, 1961.
[31] G. Li, Z. Su, M. Li, H. K. H. Lee, R. Datt, D. Hughes, C. Wang, M. Flatken, H. Köbler, J. J. Jerónimo-Rendon, R. Roy, F. Yang, J. Pascual, Z. Li, W. C. Tsoi, X. Gao, Z. Wang, M. Saliba, A. Abate, *Adv. Energy Mater.* **2022**, *12*, 2202887.
[32] I. Levine, P. K. Nayak, J. T.-W. Wang, N. Sakai, S. Van Reenen, T. M. Brenner, S. Mukhopadhyay, H. J. Snaith, G. Hodes, D. Cahen, *J. Phys. Chem. C* **2016**, *120*, 16399.
[33] L. K. Ono, S. R. Raga, S. Wang, Y. Kato, Y. Qi, *J. Mater. Chem. A* **2015**, *3*, 9074.
[34] N. Pellet, F. Giordano, M. I. Dar, G. Gregori, S. M. Zakeeruddin, J. Maier, M. Grätzel, *Prog. Photovolt.: Res. Appl.* **2017**, *25*, 942.
[35] T. J. Silverman, M. G. Deceglie, I. R. Repins, T. Zhu, Z. Song, M. J. Heben, Y. Yan, C. Fei, J. Huang, L. T. Schelhas, *IEEE J. Photovoltaics* **2023**, *13*, 740.
[36] J. Herterich, M. Unmüssig, G. Loukeris, M. Kohlstädt, U. Würfel, *Energy Technol.* **2021**, *9*, 2001104.
[37] B. Roose, *RSC Adv.* **2021**, *11*, 12095.